

Nanostructured AABB Zn (II) Phthalocyanines as Photodynamic Agents for Bacterial Inactivation

Irene Paramio, Ainhoa Salazar, Mireia Jordà-Redondo, Santi Nonell, Tomás Torres,* and Gema de la Torre*

In this work, the ability of amphiphilic Phthalocyanine (Pc) photosensitizers (PS) (Zn(II)Pcs PS1, PS2, and PS3) to assemble into cationic nanoparticles in water and to photo-inactivate bacterial strains is demonstrated. All the synthesized Zn(II)Pcs exhibit an AABB functionalization pattern, having a binaphthoxy-linked bisoindole (AA) functionalized at the chiral binaphthol core with branched (PS1) or linear (PS2 and PS3) poly-ammonium chains, and two non-functionalized isoindole rings (BB). The aggregation behavior and the stability of the nanoparticles formed by the three PS in water is studied by UV-vis, fluorescence and circular dichroism (CD) spectroscopies, and their shape and size is determined by transmission electron microscopy (TEM) and dynamic light scattering (DLS). The PS nanoparticles prove efficient in the photoinactivation of *S. aureus* and *E. coli*. Although PS2 and PS3 present better photophysical features in their monomeric form (i.e., improved singlet oxygen quantum yield), PS1 is more effective in killing both types of strains, especially the gram-negative *E. coli*. This observation may derive from the low stability found for PS1 nanoparticles, which easily disassemble after binding to the bacteria surface, recovering the photophysical properties of the non-aggregated species.

1. Introduction

Bacterial infection is still a serious threat to public health since the widespread and continual use of antibiotics has caused the generation of antibiotic-resistant bacteria.^[1] Therefore, there is an urgent need to design new efficient antimicrobial materials that act more effectively and quicker than the current antibiotics. One of the most promising methods in terms of efficiency and safety is antibacterial photodynamic therapy (aPDT),^[2–5] which produces bacterial cell death in the presence of a photosensitizer (PS), light energy of an appropriate wavelength, and molecular oxygen.^[6,7] In this treatment, PS is activated to the nanosecond-lived excited singlet state, which quickly converts to a more stable excited triplet state via intersystem crossing. The triplet PS triggers the formation of singlet molecular oxygen (¹O₂) and other reactive oxygen species (ROS) that interact with cellular components, leading to damage and even death of the microbial

cell. Porphyrinoids are the most common PS in PDT in general^[8,9] and in aPDT in particular,^[10–12] because of their singular photochemical characteristics, i.e., intense absorption in the optical therapeutic window and high triplet quantum yield. Several customized porphyrins and phthalocyanines (Pcs) functionalized with hydrophilic substituents have been synthesized and studied as PS for the inactivation of bacteria,^[9,13–15] particularly the Zn(II) complexes, due to their excellent photophysical properties and high ¹O₂ quantum yields.^[16] The rational functionalization of Zn(II)Pcs can afford both water solubility and an appropriate hydrophobicity-hydrophilicity ratio, which is relevant to drive the incorporation and intracellular localization of the PS in microorganisms. It has been demonstrated that the molecular charge of the PS is an important factor in the antibacterial activity, being cationic Pcs generally more efficient than neutral or anionic dyes due to the presence of a greater number of negative surface charges in the bacteria that attract cationic molecules.^[17] In this regard, unsymmetrically functionalized Pcs with a pronounced amphiphilic character arising from the asymmetric distribution of positively charged substituents around the Pc core is a promising strategy that has already been an object of study.^[18–23]


In the last years, numerous nanostructured PSs have been developed as a tool to enhance the therapeutic effect since they provide better biodistribution and targeting abilities than

I. Paramio, A. Salazar, T. Torres, G. de la Torre
Department of Organic Chemistry
Universidad Autónoma de Madrid
C/ Francisco Tomás y Valiente 7, Madrid 28049, Spain
E-mail: tomas.torres@uam.es; gema.delatorre@uam.es

M. Jordà-Redondo, S. Nonell
Institut Químic de Sarrià. Universitat Ramon Llull
Barcelona 08017, Spain

T. Torres
Instituto Madrileño de Estudios Avanzados (IMDEA)-Nanociencia
C/ Faraday 9, Cantoblanco, Madrid 28049, Spain

T. Torres, G. de la Torre
Institute for Advanced Research in Chemical Sciences (IADChem). Universidad Autónoma de Madrid
Madrid 28049, Spain

 The ORCID identification number(s) for the author(s) of this article can be found under <https://doi.org/10.1002/adtp.202300116>

© 2023 The Authors. *Advanced Therapeutics* published by Wiley-VCH GmbH. This is an open access article under the terms of the Creative Commons Attribution License, which permits use, distribution and reproduction in any medium, provided the original work is properly cited.

DOI: 10.1002/adtp.202300116

individual molecules. Most effort in this area has been devoted to the construction of nano-delivery systems able to encapsulate the photoactive drug,^[8,9] but these systems suffer from multi-step fabrication, and poor therapeutic outcomes associated with low drug loading. To overcome this issue, a recent strategy to form nanostructured PS, noted by some authors as the “one-for-all” approach,^[22,23] relies on the rational design of amphiphilic PS able to self-assemble into nanoparticles in the aqueous medium.^[24] If the PS are positively charged, the assembled cationic nanoparticles can be useful for application in aPDT.^[25] Also, amphiphilic cationic polymers anchored to appropriate PS can self-assemble into stable, positively charged nanoparticles.^[26,27] Both types of PDT nano-agents can strongly adhere to the negatively charged outer membranes of bacteria,^[28,29] thereby facilitating the intracellular uptake of the PS or producing the disruption of the bacterial membrane after irradiation. The latter is particularly operative for Gram-negative bacteria due to the impermeability properties of their negatively charged outer covering of phospholipids and lipopolysaccharides, which can electrostatically interact with cationic nanostructures, but make difficult the internalization of the PS.^[30,31]

Recently we have described a novel archetype of cationic, amphiphilic Pcs, **Pc-1** and **Pc-2** (**Figure 1a**),^[32] based on a binaphthylxy-linked AABB Zn(II)Pc core (with A and B coding

for differently functionalized isoindoles)^[33] holding pyridinium-substituents at the two non-bridged isoindoles. This type of Pcs showed the ability to self-assemble into positively charged, homogeneously sized nanoparticles in aqueous solutions due to their strongly marked amphiphilic character, presenting a non-polar head and the hydrophilic cationic tail. As the Pc macrocycle is not completely surrounded by positive charges, the latter can be accommodated with minimal electrostatic repulsion when the aromatic cores stack due to solvophobic interactions. These cationic Zn(II)Pc nanoparticles with cancelled photophysical properties exhibited strong binding to the negative outer membrane of Gram-positive and Gram-negative bacteria, and subsequent disassembly of the nanoparticles rendered an efficient inactivation of both types of bacteria upon light irradiation. Compared to other tetracationic pyridinium PS, the self-assembly behavior of this type of PS provides them with much stronger aPDT activity both in terms of concentration of the PS and light dose.

Encouraged by these results, we have undertaken the synthesis and aPDT studies of three new PS (**Figure 1b**) based on the binaphthylxy-linked AABB Zn(II)Pc structure functionalized with other different polycationic residues that provide amphiphilicity and self-assembly ability in aqueous media. In this case, the positive charges have been introduced by quaternization

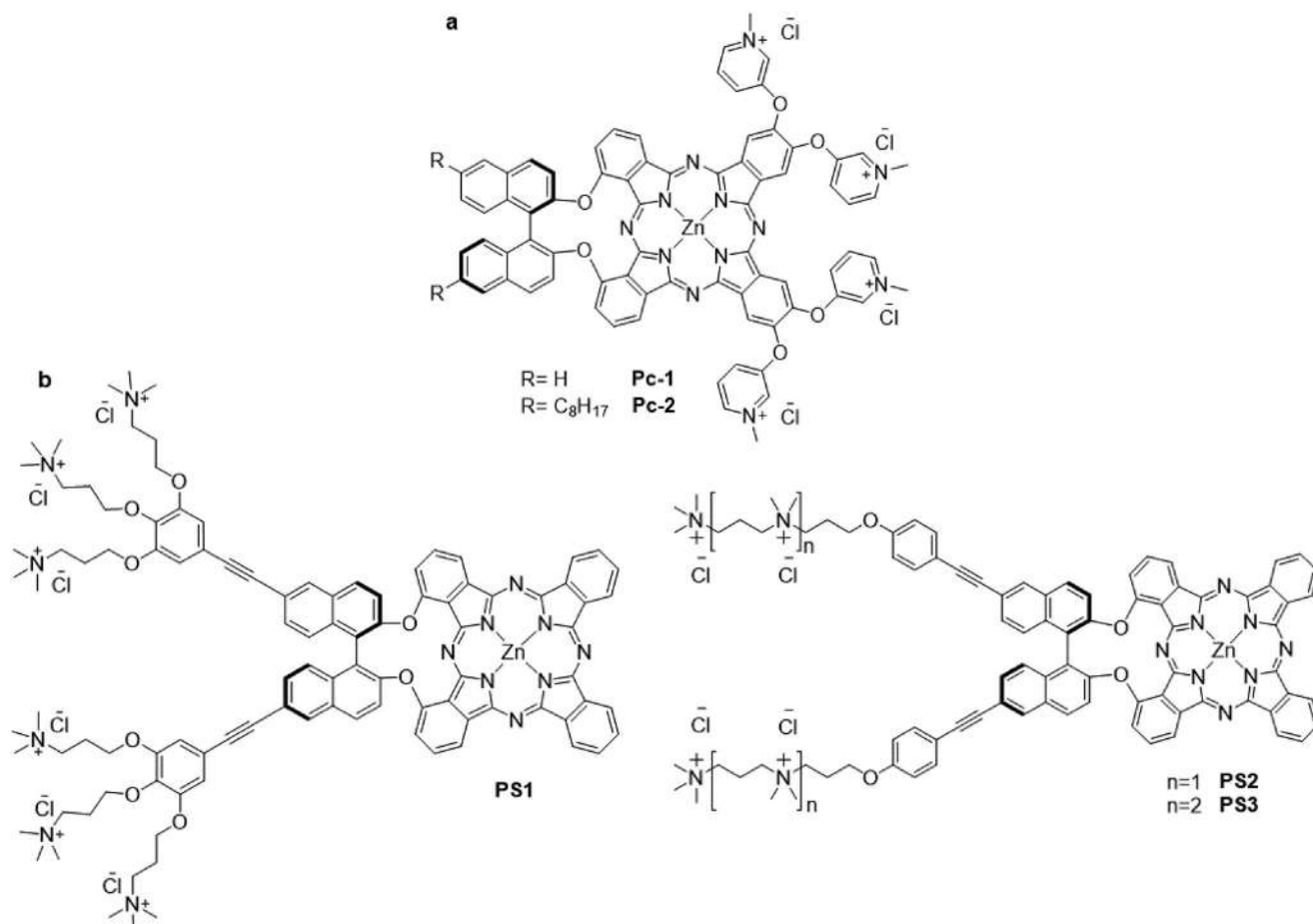


Figure 1. Structure of AABB-Zn(II)Pcs a) **Pc-1** and **Pc-2**, previously reported,^[27] and b) **PS1**, **PS2**, and **PS3**, studied in this work.

of either linear or branched polyamine chains linked to the binaphthol core. The aim of the work is to determine the influence that the position of the hydrophilic chains in this type of AABB Zn(II)Pcs, as well as the nature and number of positive charges, exerts on i) the self-assembly behavior in aqueous solutions and the stability of the positively charged nanostructures obtained; ii) the uptake by Gram-positive and Gram-negative bacteria; and iii) the efficiency in killing both types of microorganisms.

2. Results and Discussion

2.1. Synthesis

As mentioned above, the binaphthyl-Zn(II)Pc core has been functionalized with three different polycationic chains, aiming at exploring the effect of the different distribution and number of positively charged groups on the aggregation abilities and aPDT outcomes of this type of PS. In the case of **PS1**, branched ammonium chains are attached to the binaphthol unit, whereas for **PS2** and **PS3**, four and six ammonium moieties, respectively, are distributed linearly along the chain.

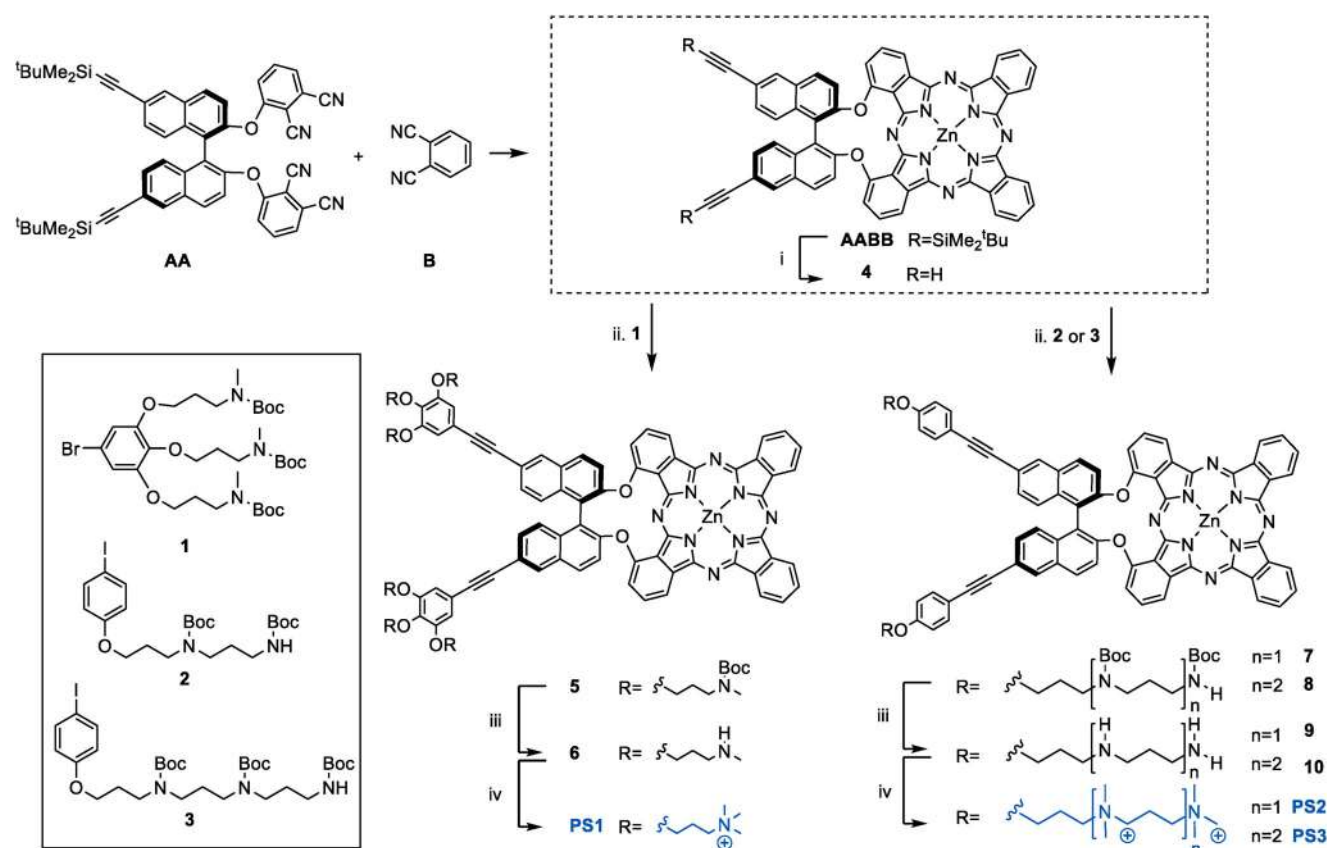
Therefore, for the preparation of the PS, we first tackled the synthesis of the corresponding polyamine chains **1–3** (Scheme 1). All of them were prepared using *N*-Boc protected, mesylated amino-alcohol units, either used for the alkylation of 5-bromobenzene-1,2,3-triol (for **1**) or as starting material for successive alkylation reactions to obtain the *N*-Boc protected ligands

2 and **3**. Synthetic details on the preparation of these derivatives are provided in the Supporting Information.

The three PS were prepared starting from a common Zn(II)Pc intermediate (**AABB**, Scheme 1), which was synthesized by mixed condensation between non-functionalized phthalonitrile **B** and a geometrically constrained binaphthoxy-bridged bisphthalonitrile **AA** holding two protected acetylenes, following previously reported conditions that favor the formation of the targeted compound in high yield (i.e., 30%).^[33] After deprotection of **AABB** using TBAF, the resulting Zn(II)Pc **4** was used in the next reactions without further purification due to its instability.

For the preparation of **PS1**, **4** was reacted with **1** under copper-free, Sonogashira coupling conditions, using Pd(PPh₃)₄ as a catalyst. Zn(II)Pc **5** was isolated in 40% yield from a reaction mixture that also contains the mono-coupled product. Then, cleavage of the *tert*-butyloxycarbonyl protecting groups with TFA, followed by quaternization of the amines with MeI and subsequent counterion exchange (i.e., iodides by chlorides) yielded the water-soluble **PS1** in 85% yield.

The synthesis of **PS2** and **PS3** was also carried out by Sonogashira coupling of **4** with **2** and **3**, respectively, under similar conditions, rendering **7** (54% yield) and **8** (65% yield). Also in these cases, deprotection of the *tert*-butyloxycarbonyl protecting groups, quaternization of the amines with MeI, and subsequent counterion exchange led to the targeted PS. The compounds were characterized by ¹H-NMR, ¹³C-NMR, IR and HR-MS. The strong aggregation of the PS at the concentration necessary to record



Scheme 1. Synthetic route toward **PS1**, **PS2**, and **PS3**; i) TBAF in THF, 0 °C to rt for 2 h; ii) Pd(PPh₃)₄ in DMF:Et₃N 2:1, 80 °C; iii) TFA in DCM, rt for 6 h, iv) MeI and 1,2,2,6,6-pentamethylpiperidine (PMP) in DMF at rt for 16 h, then Dowex resin in MilliQ water for 2 h.

Table 1. Photophysical data of **PS1**, **PS2**, and **PS3** in DMSO.

	$\log \epsilon (\lambda)$	$\Phi_F^a)$	$\Phi_\Delta^b)$	$\tau_F / \text{ns}^c)$	$\tau_T / \mu\text{s}$	$\tau_\Delta / \mu\text{s}^d)$
PS1	4.8 (330), 5.2 (680)	0.09 ± 0.04	0.43 ± 0.02	2.80 ± 0.021	0.92 ± 0.07	4.85 ± 0.16
PS2	4.4 (338), 5.0 (680)	0.13 ± 0.01	0.61 ± 0.10	2.90 ± 0.021	1.16 ± 0.18	5.17 ± 0.08
PS3	4.4 (337), 5.0 (680)	0.13 ± 0.01	0.64 ± 0.05	2.89 ± 0.001	0.95 ± 0.09	5.27 ± 0.07

^{a)} λ_{exc} : 640 nm; ^{b)} λ_{exc} : 660 nm; λ_{obs} : 1275 nm; ^{c)} λ_{exc} : 654 nm; λ_{obs} : 690 nm; ^{d)} air-saturated

Table 2. Photophysical data of **PS1**, **PS2**, and **PS3** in water.

	$\log \epsilon (\lambda)$	$\Phi_F^a)$	$\Phi_\Delta^b)$	$\tau_F / \text{ns}^c)$	$\tau_T / \mu\text{s}^d)$	$\tau_\Delta / \mu\text{s}^d)$
PS1	4.9 (329), 4.7 (632), 4.5 (671)	0.002	0.06	2.88 ± 0.013	4.4 ± 0.6	64.6 ± 1.6
PS2	4.0 (336), 3.9 (633), 3.8 (676)	<0.0001	0.04	2.45 ± 0.029	7.8 ± 0.8	52.4 ± 1.6
PS3	4.4 (336), 4.3 (633), 4.3 (685)	<0.0001	0.03	2.67 ± 0.021	5.4 ± 0.5	65.0 ± 1.6

^{a)} λ_{exc} : 640 nm; ^{b)} in D₂O; λ_{exc} : 660 nm; λ_{obs} : 1275 nm; ^{c)} λ_{exc} : 654 nm; λ_{obs} : 690 nm; ^{d)} in air-saturated D₂O

¹H-NMR (>0.006 M in dimethylsulfoxide (DMSO)) rendered poorly resolved spectra, especially for **PS2** and **PS3**, but the structure of the compounds was confirmed by HR-MS (see Supporting Information).

Hexacationic **PS1** and **PS3** proved perfectly soluble in pure water, while tetracationic **PS2** had to be injected from DMSO into water to obtain aqueous solutions (1% DMSO final content). The stability of the PS in biological-like medium (i.e., PBS) was studied by UV-vis absorption (Figure S54, Supporting Information). **PS1** and **PS3** proved very stable for long periods, while **PS2** showed lower stability, probably due to the necessary presence of DMSO in the final solution.

2.2. Photophysical Characterization and Aggregation Studies

A compilation of the photophysical data for **PS1**, **PS2**, and **PS3** can be found in **Table 1** and **Table 2**. Initially, ground-state absorption experiments were performed in DMSO, a coordinative solvent that prevents the stacking of Zn(II)Pcs. The absorption spectra for all PS reveal the typical Q band for monomeric species and the B band transition at ≈ 680 and 330 nm, respectively. For the verification of the Lambert–Beer law, an analysis of linear regression between the intensity of the Q and Soret bands and the concentration of the PS showed determination coefficient (R^2) values close to 1, which confirmed the lack of aggregation in this solvent (**Figure 2**; Figures S49 and S51, Supporting Information) at

the studied range of concentration. All compounds showed similar molar absorption coefficients, but the fluorescence quantum yields (Φ_F) of both structurally related **PS2** and **PS3** are $\approx 40\%$ larger than for **PS1**. Singlet oxygen quantum yields (Φ_Δ) were determined by direct observation of its characteristic phosphorescence at 1275 nm. Again, **PS2** and **PS3** show similar values ($\Phi_\Delta = 0.61$ and 0.64, respectively), $\approx 40\%$ larger than that of **PS1** ($\Phi_\Delta = 0.43$).

As previously observed with related cationic Pc amphiphiles,^[32] the high directional amphiphilic character of **PS1**, **PS2**, and **PS3** should drive the formation of aggregates in aqueous media to reduce the solvation energy. Although electrostatic repulsion between positive charges could hamper the aggregation, the asymmetric distribution of the cationic substituents around the central Pc core may allow these aromatic molecules to aggregate through π - π stacking with minimum repulsive interactions.

Therefore, UV-vis and fluorescence emission spectroscopies were first used to study the aggregation of **PS1**, **PS2**, and **PS3** in aqueous media (**Figure 3a**; Figure S53, Supporting Information). Upon increasing the percentage of water in DMSO:water solutions of the three PS, a progressive reduction in the intensity of the Q-bands was observed in the absorption spectra, together with the onset of a new band at ≈ 630 nm in each case, which is typical for the formation of H-type aggregates. In turn, a small increase in fluorescence intensity was observed for **PS1** and **PS3**

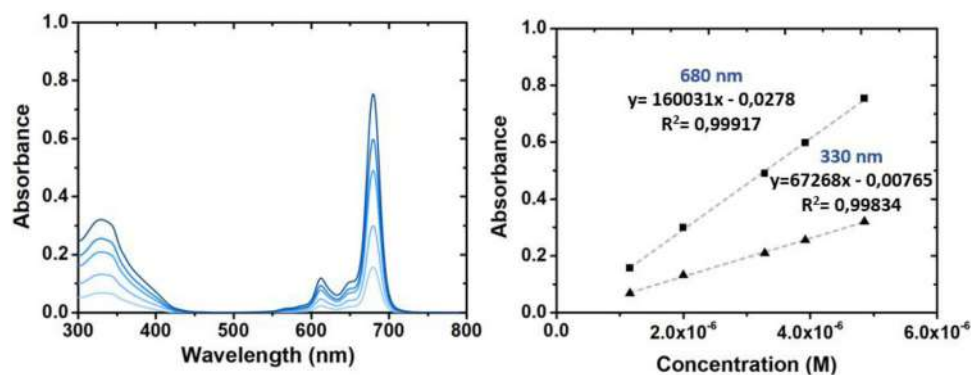


Figure 2. Absorption studies with **PS1** in DMSO at a range of concentrations (from 1×10^{-6} M to 5×10^{-6} M).

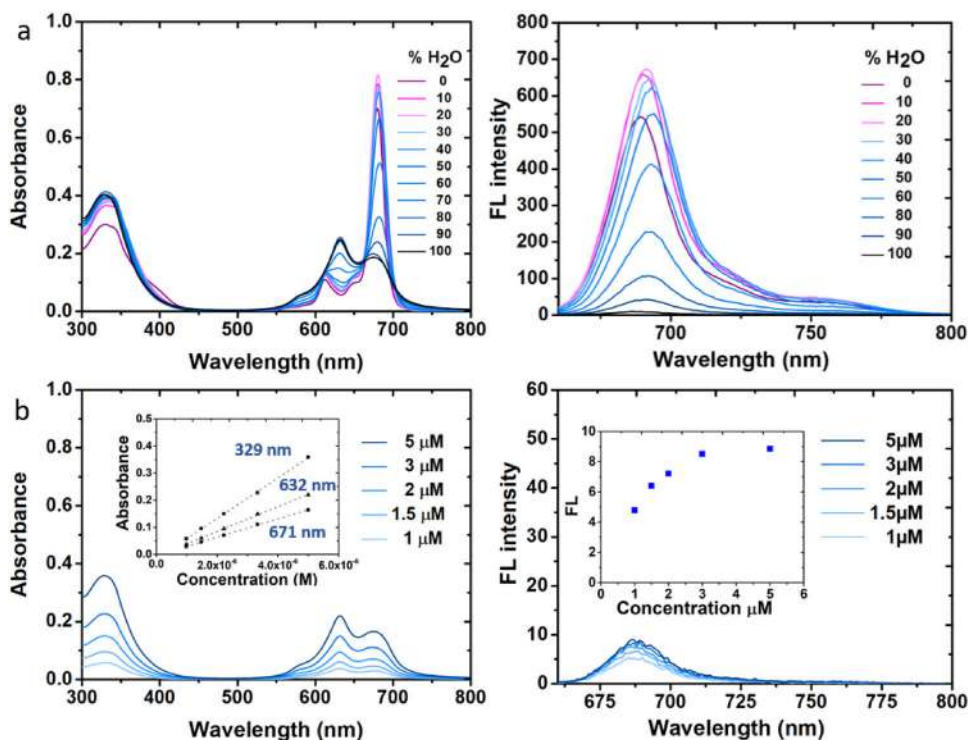


Figure 3. a) Absorption (left) and fluorescence (right) spectral changes upon increasing the water percentage in solutions of PS1 (5×10^{-6} M) in DMSO: water mixtures; b) Absorption and fluorescence spectra of PS1 in water at different concentrations (from 1×10^{-6} M to 5×10^{-6} M).

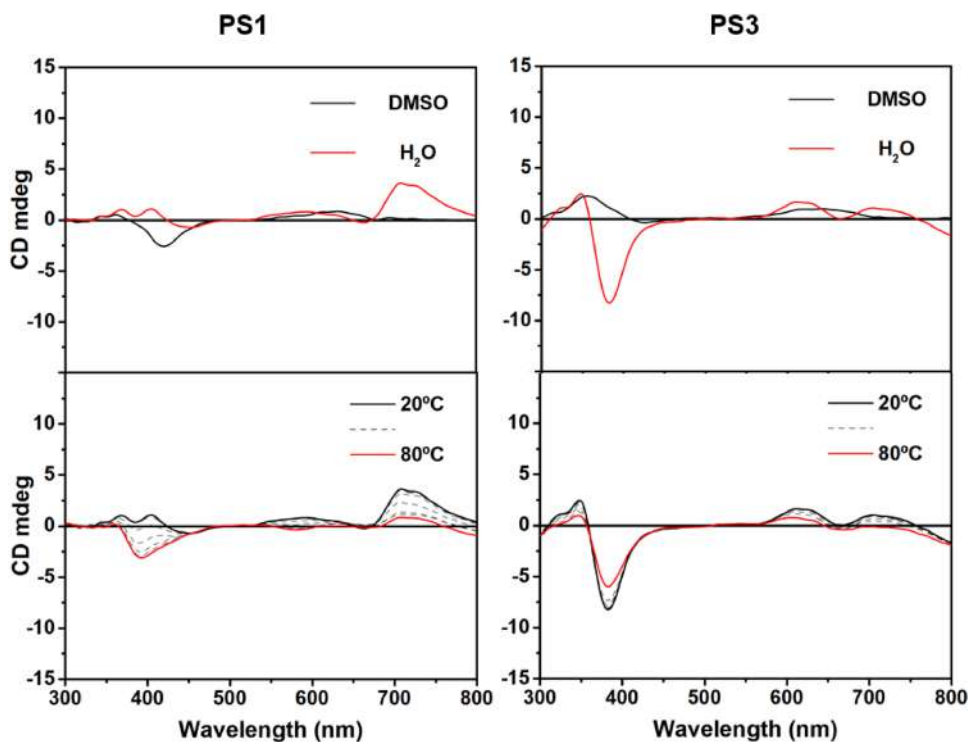


Figure 4. CD spectra of PS1 and PS3 in DMSO and water (top), and temperature studies from 20 to 80 °C at a concentration of 6×10^{-5} M.

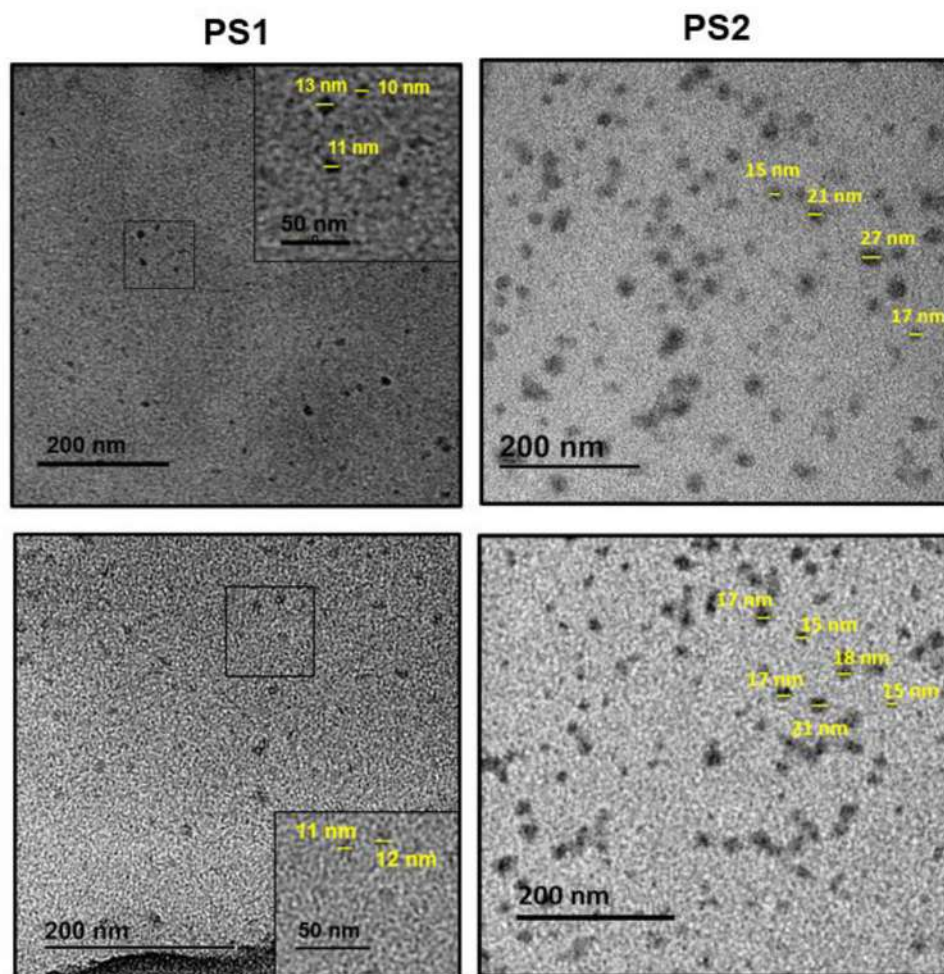


Figure 5. TEM images of **PS1** and **PS2** prepared from water solutions (8×10^{-5} M).

when adding up to 20% water (up to 10% water for **PS2**), which is likely due to a change in the solvation sphere of the molecules. At higher water content, a progressive decrease in the intensity of fluorescence was observed for all PS, which is consistent with the hypothesis of *H*-type aggregation.

The fluorescence and singlet oxygen quantum yields of **PS1**, **PS2**, and **PS3** in pure water were then determined. As expected, a dramatic decrease in the fluorescence and singlet oxygen quantum yields with respect to DMSO solutions was observed for all the compounds, consistently with the aggregation-promoted self-quenching (Table 2). Nevertheless, fluorescence and singlet oxygen decays could still be observed with similar lifetimes as in DMSO, albeit with ≈ 20 -fold less intensity (Figure S61, Supporting Information). This behavior may suggest that the aggregates are in equilibrium with monomeric species, which are responsible for the residual fluorescence and singlet oxygen signals observed. The higher fluorescence intensity of **PS1** relative to **PS2** and **PS3** suggests that the concentration of monomers is higher for **PS1**.

Next, we performed concentration-dependent fluorescence and absorption experiments in water solutions (Figure 3b) to ascertain the behavior of the aggregates. As previously observed

for **Pc-1** and **Pc-2**,^[32] the fluorescence intensity of **PS1**, **PS2** and **PS3** in water increases up to a plateau value when increasing their concentration (Figure 3b; Figures S50 and S52, Supporting Information), in agreement with the hypothesis of fluorescent monomers in equilibrium with non-fluorescent aggregates (Figure S55, Supporting Information). Also consistent with this hypothesis is that the intensity of the Q bands in the absorption spectra of the three PS increases linearly with concentration, but the shape and relative intensity of the monomer/aggregate absorptions remain the same. We hypothesize that discrete micelle-like nanostructures start to form at very low concentrations. Their size is kept constant owing to the strong contribution of the electrostatic repulsions between positive charges, which does not allow for continuous growth. The effect of increasing the concentration is merely to increase the number of nanoaggregates as usually observed for micellization of surfactants.^[34]

The presence of the chiral (*R* enantiomer) binaphthol unit in **PS1**, **PS2**, and **PS3** not only governs the preparation of these unsymmetric AABB-type Pcs (not easily obtained by other means), but also permits to study the self-assembly process of these molecules following the changes in circular dichroism (CD)

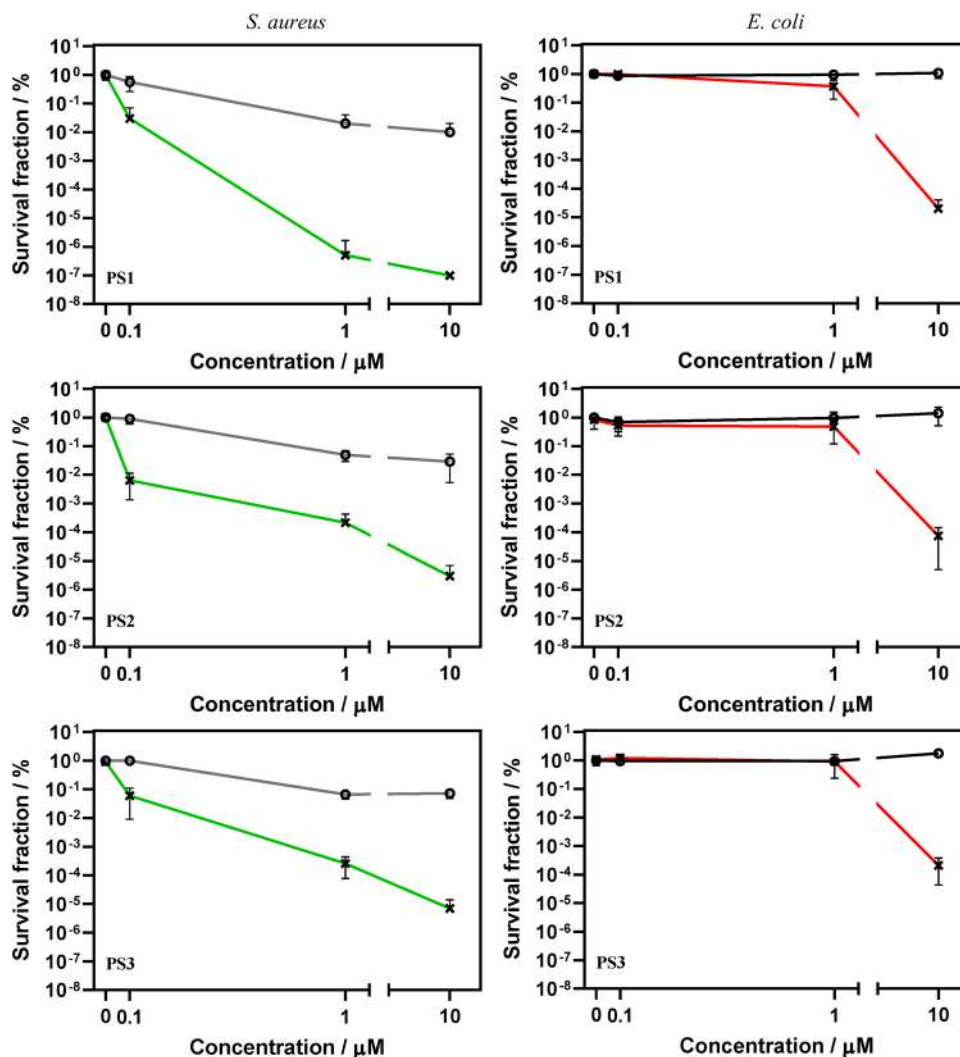


Figure 6. Photoinactivation of *S. aureus* (left) and *E. coli* (right) in PBS using PS1 (top), PS2 (middle), and PS3 (bottom) incubated for 30 min and irradiated with 30 J cm⁻² of red light ($\lambda = 660 \text{ nm} \pm 10 \text{ nm}$). Light-treated samples are shown in crosses and dark controls in circles. Data correspond to the mean \pm SD after performing three replicates.

spectra. In DMSO solutions, where aggregation does not take place, CD signals with low intensity appear in the Soret and Q band region for all PS (Figure 4; Figure S56, Supporting Information). On the other hand, in aqueous solutions, we could observe the appearance of two new broad signals around 600 and 700 nm that correlate with those appearing in the UV absorption spectra in water. In addition, a change in the sign and intensity of the bands in the Soret region was discernible. All these changes can be assigned to the formation of chiral aggregated species. To check the stability of the aggregates, water solutions of each PS were heated up to 80 °C and the CD signal was recorded. While the CD signals of PS2 and PS3 remained almost unchanged, the CD of PS1 changed to almost reach the spectrum of the non-aggregated monomeric species in pure DMSO, which suggests a lower stability of PS1 aggregates, probably due to the higher steric hindrance and higher contribution of the electrostatic repulsions between the branched polyammonium chains that destabilize the supramolecular structure.

Next, we turned to study the aggregates formed in aqueous solution by TEM microscopy. MilliQ water solutions of each PS at different concentrations were prepared and deposited over specific grids. All PS aggregate into small spherical particles in the 10–25 nm range (Figure 5; Figure S57, Supporting Information), similarly as observed previously for Pc1 and Pc2.^[32] DLS experiments were also performed over all molecules, and the results were consistent with the observed sizes in TEM images (Figures S58–S60, Supporting Information). In addition, the zeta potential of the nanoparticles was measured to determine their surface charge and dispersion stability. The higher the potential magnitude exhibited by the nanoparticles, the larger the electrostatic repulsion and, therefore, increased stability. The zeta potential measured by DLS is $+18 \pm 5 \text{ mV}$ for PS1, $+24 \pm 6 \text{ mV}$ for PS2 and $33 \pm 11 \text{ mV}$ for PS3. These results account for lower stability of PS1 nanoparticles, in agreement with the variable temperature CD experiments.

Table 3. Z-potential studies of *S. aureus* and *E. coli* in water using **PS1**, **PS2** and **PS3** at a concentration of 10 μM .

	<i>S. aureus</i>	<i>E. coli</i>
Control	-20 ± 3	-32 ± 3
PS1	-3 ± 3	$+2 \pm 2$
PS2	$+2 \pm 2$	-1 ± 2
PS3	$+9 \pm 3$	$\approx 0 \pm 2$

2.3. Antimicrobial In Vitro Studies

To evaluate the functionality of the cationic nanoparticles as feasible photo-antibacterial products, they were tested against *Staphylococcus aureus* and *Escherichia coli*, as representative examples of Gram-positive and Gram-negative bacteria, respectively. Contrary to previous results with polymer electrolytes with terminal quaternary ammonium groups, the bactericidal activity in the dark of the three PS was negligible, especially for *E. coli*. However, we found that 1 μM **PS1** was able to efficiently photo-inactivate *S. aureus*, reducing the population by more than 6 \log_{10} (99.9999%) after exposure to 30 J cm^{-2} of red light (**Figure 6**). Compounds **PS2** and **PS3** showed lower phototoxicity against *S. aureus*, nevertheless killing 3 \log_{10} under the same conditions. Regarding *E. coli*,

all compounds needed a concentration of at least 10 μM to achieve a 4 \log_{10} reduction at 30 J cm^{-2} of red light. These results are consistent with the generally accepted notion that Gram-negative bacteria are more difficult to photo-inactivate than Gram-positive due to their double membrane.^[4] Intriguingly, **PS1** was found to be slightly more efficient than **PS2** and **PS3**. This result is, at first sight, surprising in view of: i) its 40% lower singlet oxygen quantum yield; and ii) the less-positive zeta-potential of its nanoaggregates, which would suggest less-efficient electrostatic binding of **PS1** nanoparticles to the negatively-charged bacteria.

2.4. Interaction of the PSs with the Bacteria

To resolve this issue, the zeta potential of both bacteria was measured before and after adding 10 μM PS. Unbound PS aggregates were eliminated by two cycles of centrifugation and resuspension in neat water before the measurements. As shown in **Table 3**, incubation with the nanoparticles caused large changes in zeta potential for both types of bacteria, which indicates extensive surface binding. **PS2** and **PS3** show the highest binding to *S. aureus* while no appreciable differences in binding can be observed for *E. coli*. Thus, the higher photoinactivation efficiency of **PS1** against *S. aureus* and *E. coli* does not correlate with the extent of bacterial binding, as indicated by the change of zeta potential.

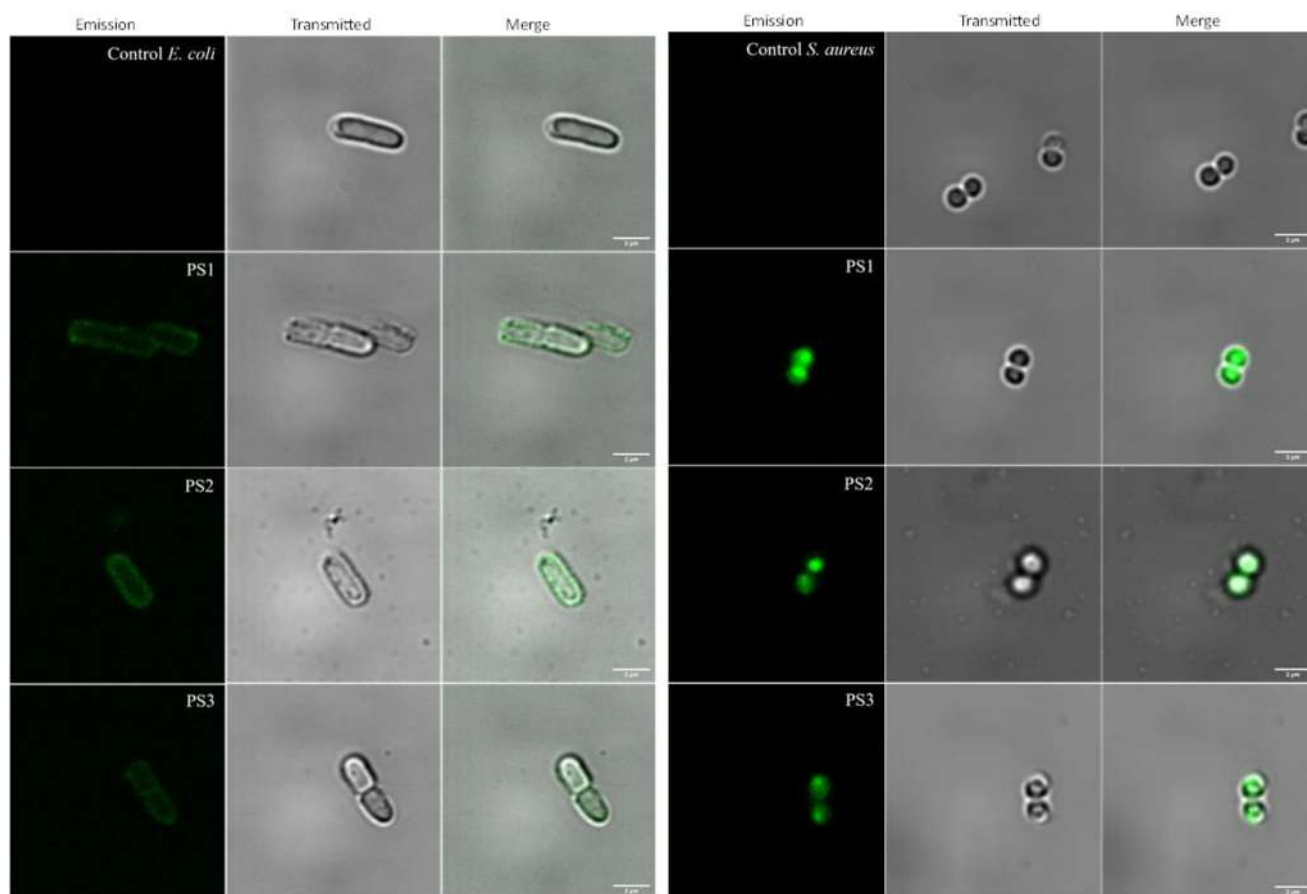


Figure 7. Confocal images of *E. coli* (left) and *S. aureus* (right) bacteria incubated for 10 min with **PS1**, **PS2**, and **PS3** 50 μM . Non-treated bacteria were used as controls.

In view of the previous observations, the most likely explanation for the different inactivation abilities of the three PS is that, after binding to the surface of the bacteria, **PS1** nanoparticles disassemble into **PS1** monomers more effectively than **PS2** and **PS3**, giving rise to a better photophysical activity. This is consistent with the lower stability of the **PS1** nanoaggregates and would explain its higher photo-antimicrobial efficiency.

The interaction between bacteria and the PSs was investigated by confocal laser scanning microscopy, which clearly showed the fluorescence of the PSs associated with the bacteria (**Figure 7**), confirming their disassembly. The images indicate that all **PSs** are internalized by *S. aureus* but accumulate in the cell wall of *E. coli*, which is consistent with the respective complexity of their cell walls and the differences in their photoinactivation efficiency.^[35]

3. Conclusion

In this work, we have validated our recent approach toward the preparation of efficient PS for bacteria inactivation, which relies on the synthesis of cationic, amphiphilic molecules based on binaphthoxy-linked AABB Zn(II)Pcs able to organize in nanostructures with improved transport properties and strong interactions with the bacterial outer membrane. Founding experiments performed with **Pc1** and **Pc2** holding pyridyloxy substituents at the isoindoles (**Figure 1**)^[32] indicated that these molecules self-assemble into positively charged, homogeneously sized nanoparticles in aqueous solutions that render an efficient inactivation of Gram-positive and Gram-negative bacteria upon light irradiation because of the strong electrostatic interactions between the positive particles and the negative bacteria surface. The herein-reported PS (**PS1**, **PS2**, and **PS3**) represent a modification of the formerly reported hydrophilic/hydrophobic distribution around the Pc skeleton. The introduction of hydrophilic chains at the binaphthol ring has also led to Zn(II)Pcs being able to form spherical nanoaggregates in water, rather uniform in shape and size. However, zeta-potential values and temperature-dependent studies in solution indicate that the stability of the nanoparticles formed by **PS1** is moderate.

The self-assembly of the three Pc amphiphiles is driven by the amphiphilic character, but the growth of the nanoparticles is certainly impeded by the bulkiness and rigidity of the binaphthol core and the electrostatic repulsion between charges. In the case of **PS1**, the branched chains occupy a larger space around the Pc core, which makes more difficult the stacking of neighboring aromatic cores prompted by the solvophobic interactions. This feature makes the difference between the self-assembly behavior of **PS1**, and **PS2/PS3**, the latter forming larger and more stable assemblies in which charges at the linear polyammonium chains are better accommodated.

More than a drawback, the lower stability of **PS1** nanoparticles seems advantageous since it allows for an effective disassembly of the Zn(II)Pc components of the nanoparticle after bacterial uptake, yielding photophysically active PS molecules that efficiently kill *S. aureus* and, to a lesser extent, *E. coli*. From these results, it could be concluded that an appropriate assembly/disassembly equilibrium may improve the performance of the nanomedicines built by the self-assembly of amphiphilic PS.

Supporting Information

Supporting Information is available from the Wiley Online Library or from the author.

Acknowledgements

I.P., A.S., and M.J.-R. contributed equally to this work. The authors gratefully acknowledge financial support from the Spanish AEI through grants PID2020-116490GB-I00, PID2020-115801RB-C21, and PID2020-115801RB-C22. The authors also thank financial support to the Comunidad de Madrid and the Spanish State through the Recovery, Transformation and Resilience Plan [“Materiales Disruptivos Bidimensionales (2D)” (MAD2D-CM) (UAM1)-MRR Materiales Avanzados], and the European Union through the Next Generation EU funds. IMDEA Nanociencia acknowledges support from the “Severo Ochoa” Program for Centers of Excellence in R&D (MINECO, Grant SEV2016-0686). S.N. thanks the Departament de Recerca i Universitats de la Generalitat de Catalunya for the support given to the research group (2021 SGR 01023) and the ICREA-Catalan Institution for Research and Advanced Studies for grant No. Ac2232308.

Conflict of Interest

The authors declare no conflict of interest.

Data Availability Statement

The data that support the findings of this study are available from the corresponding author upon reasonable request.

Keywords

amphiphiles, nanoparticles, photodynamic inactivation, phthalocyanines, self-assembly

Received: April 6, 2023

Revised: July 3, 2023

Published online: August 27, 2023

- [1] K. Bush, P. Courvalin, G. Dantas, J. Davies, B. Eisenstein, P. Huovinen, G. A. Jacoby, R. Kishony, B. N. Kreiswirth, E. Kutter, S. A. Lerner, S. Levy, K. Lewis, O. Lomovskaya, J. H. Miller, S. Mobashery, L. J. V. Piddock, S. Projan, C. M. Thomas, A. Tomasz, P. M. Tulkens, T. R. Walsh, J. D. Watson, J. Witkowski, W. Witte, G. Wright, P. Yeh, H. I. Zgurskaya, *Nat. Rev. Microbiol.* **2011**, *9*, 894.
- [2] M. Hamblin, *Curr. Opin. Microbiol.* **2016**, *33*, 67.
- [3] F. Cieplik, D. Deng, W. Crielaard, W. Buchalla, E. Hellwig, A. Al-Ahmad, T. Maisch, *Crit. Rev. Microbiol.* **2018**, *44*, 571.
- [4] M. Wainwright, T. Maisch, S. Nonell, K. Plaetzer, A. Almeida, G. P. Tegos, M. R. Hamblin, *Lancet Infect. Dis.* **2017**, *17*, 49.
- [5] G. Jori, C. Fabris, M. Soncin, S. Ferro, O. Coppellotti, D. Dei, L. Fantetti, G. Chiti, G. Roncucci, *Lasers Surg Med* **2006**, *38*, 468.
- [6] G. Jori, M. Camerin, M. Soncin, L. Guidolin, O. Coppellotti, in *Photodynamic Inactivation of Microbial Pathogens: Medical and Environmental Applications*, Vol. 11 (Eds: M. R. Hamblin, G. Jori), The Royal Society of Chemistry, London **2011**.
- [7] M. Ethirajan, Y. Chen, P. Joshi, R. K. Pandey, *Chem. Soc. Rev.* **2011**, *40*, 340.
- [8] V. Almeida-Marrero, E. van de Winkel, E. Anaya-Plaza, T. Torres, A. de la Escosura, *Chem. Soc. Rev.* **2018**, *47*, 7369.

- [9] P. C. Lo, M. S. Rodríguez-Morgade, R. K. Pandey, D. K. P. Ng, T. Torres, F. Dumoulin, *Chem Soc Rev* **2020**, *49*, 1041.
- [10] N. Malatesti, I. Munitic, I. Jurak, *Biophys. Rev.* **2017**, *9*, 149.
- [11] L. Sobotta, P. Skupin-Mrugalska, J. Piskorz, J. Mielcarek, *Eur. J. Med. Chem.* **2019**, *175*, 72.
- [12] B. M. Amos-Tautua, S. P. Songca, O. S. Oluwafemi, *Molecules* **2019**, *24*, 2456.
- [13] A. Galstyan, *Chem. - Eur. J.* **2021**, *27*, 1903.
- [14] A. Galstyan, U. Dobrindt, *J. Mater. Chem. B* **2018**, *6*, 4630.
- [15] M. B. Spesia, E. N. Durantini, *Chem. Rec.* **2022**, *22*, 202100292.
- [16] J. C. H. Chu, M. L. Chin, C. T. T. Wong, M. Hui, P.-C.h. Lo, D. K. P. Ng, *Adv. Ther.* **2021**, *4*, 2000204.
- [17] C. P. S. Ribeiro, L. M. O. Lourenço, *J. Photochem. Photobiol. C* **2021**, *48*, 100422.
- [18] M. A. Revuelta-Maza, P. González-Jiménez, C. Hally, M. Agut, S. Nonell, G. de la Torre, T. Torres, *Eur. J. Med. Chem.* **2020**, *187*, 111957.
- [19] B. G. Ongarora, X. Hu, H. Li, F. R. Fronczek, M. G. H. Vicente, *Med-ChemComm* **2012**, *3*, 179.
- [20] Y. Ikala, O. Babu, T. Nyokong, *Photodiagnosis Photodyn Ther* **2022**, *38*, 102863.
- [21] H. Lin, J. Chen, Y. Zhang, A. Ulla, J. Liu, F. Lin, L. Jiang, M. Huang, *J. Inorg. Biochem.* **2018**, *189*, 192.
- [22] X. Li, D. Lee, J.-D. Huang, J. Yoon, *Angew. Chem., Int. Ed.* **2018**, *130*, 10033.
- [23] E. Lee, X. Li, J. Oh, N. Kwon, G. Kim, D. Kim, J. Yoon, *Chem. Sci.* **2020**, *11*, 5735.
- [24] J.-J. Hu, Q. Lei, X.-Z. Zhang, *Prog. Mat. Sci.* **2020**, *114*, 100685.
- [25] J. Li, W. Sun, Z. Yang, G. Gao, H.-H. Ran, K.-F. Xu, Q.-Y. Duan, X. Liu, F.-G. Wu, *ACS Appl. Mater. Interfaces* **2020**, *12*, 54378.
- [26] Y.-D. Sun, Y.-X. Zhu, X. Zhang, H.-R. Jia, Y. Xia, F.-G. Wu, *Langmuir* **2019**, *35*, 14324.
- [27] H.-R. Jia, Y.-X. Zhu, Z. Chen, F.-G. Wu, *Appl. Mater. Interfaces* **2017**, *9*, 15943.
- [28] A. C. Tedesco, F. L. Primo, P. d. C. C. de Jesus, in *Multifunctional Systems for Combined Delivery, Biosensing and Diagnostics* (Ed: A. Grumezescu), Elsevier, New York **2017**.
- [29] I. Paramio, T. Torres, G. de la Torre, *ChemMedChem* **2021**, *16*, 2441.
- [30] X. Zhen, L. Chudal, N. K. Pandey, J. Phan, X. Ran, E. Amador, X. Huang, O. Johnson, Y. Ran, W. Chen, M. R. Hamblin, L. Huang, *Mater. Sci. Eng. C* **2020**, *110*, 110659.
- [31] L. Huang, L. Ma, W. Xuan, X. Zhen, H. Zheng, W. Chen, M. R. Hamblin, *J. Biomed. Nanotechnol.* **2019**, *15*, 2142.
- [32] M. A. Revuelta-Maza, E. de las Heras, M. Agut, S. Nonell, T. Torres, G. de la Torre, *Chem. - Eur. J.* **2021**, *27*, 4955.
- [33] M. A. Revuelta-Maza, T. Torres, G. de la Torre, *Org. Lett.* **2019**, *21*, 8183.
- [34] W. Al-Soufi, M. A. Novo, *Molecules* **2021**, *26*, 5339.
- [35] Y. Wang, S. D. Jett, J. Crum, K. S. Schanze, E. Y., D. G. Whitten, *Langmuir* **2013**, *29*, 781.